MODELING TURBULENT COUETTE FLOW IN A PLANE CHANNEL

B. L. Rozhdestvenskii, I. N. Simakin,
and M. I. Stoinov

UDC 532.516:532.574.4

Turbulent Couette flow in a plane channel at transitional Reynolds numbers is modeled by numerical integration of the Navier–Stokes equations for a viscous incompressible liquid. The friction coefficient, mean velocity profile, Reynolds stress, and certain average characteristics of the calculated three-dimensional secondary static-stationary flows agree well with the corresponding characteristics of real turbulent flows. The instability of laminar Couette flow relative to finite amplitude three-dimensional perturbations is established.

1. We will consider the pressure-free flow of a viscous incompressible liquid in an infinite plane channel, the walls of which move at constant velocity in opposite directions (planar Couette flow). Stability of a laminar Couette flow relative to infinitely small perturbations has been studied exhaustively (see the review [1]). In particular, stability has been strictly proven for infinitely small perturbations at arbitrary Reynolds number [2]. On the other hand, it has been established experimentally that at $R \gtrsim 10^3$* disruption of the laminar flow regime with transition to turbulence can occur [3, 4]. This experimental fact has been related to instability of the flow in question relative to finite amplitude perturbations.

When methods of the nonlinear theory of hydrodynamic stability are used to study stability of Couette flow serious difficulties arise, related to the absence of a neutral curve. The majority of studies have considered two-dimensional Navier–Stokes equations [5-10]. The critical Reynolds numbers obtained in [5-8] differ from each other by an order of magnitude and more. The results of [9, 10] indicate stability of Couette flow relative to two-dimensional finite perturbations.

Turbulent Couette flow was modeled by numerical integration of the Navier–Stokes equations in [11-14]. At R = 5000 [11] found that two-dimensional finite amplitude perturbations decay. All calculations of three-dimensional flows were performed over very brief time intervals. Calculations were completed at the stage of abrupt increase in perturbation amplitude, while the mean velocity profiles differed only insignificantly from the laminar case. It is clear that one cannot speak of establishment of any secondary flow regime here. In [12] the authors studied behavior over time of a perturbation in the form of a superposition of a finite amplitude two-dimensional and a small three-dimensional perturbation. It developed that at $R \gtrsim 10^3$ the three-dimensional perturbations increase exponentially while the two-dimensional decay. As before, calculations were performed over small time intervals. In [13] three-dimensional flow as modeled at R = 1450. In the calculations the pulsation energy oscillated with a remarkably high amplitude, while the velocity profile had an anomalous form (the sign of the velocity changed at three points). Apparently this was related to the fact that an insufficient number of base functions were used in representing the approximate solution. We will also note [14], which performed modeling of turbulent Couette flow at R = 750-1750. At all Reynolds numbers considered, three-dimensional secondary flows were obtained. The calculated profiles of velocity and intensity of mean-square velocity pulsations agreed qualitatively with experiment. Yet for a significant number of important characteristics there was significant disagreement with experimental data: Reynolds stress distribution in the central portion of the channel was inhomogeneous, the mean velocity profile did not agree with a logarithmic profile, and the friction coefficient was significantly lower than experiment.

2. The present study will investigate stability of Couette flow relative to finite perturbations, and model secondary static-stationary flows which can be compared to the turbu

*Here and below, $R = U_w h/\nu$, where U_w is the speed of the walls, h is the channel half-width, and ν is the kinematic viscosity coefficient.

Moscow. Translated from Zhurnal Prikladnoi Mekhaniki i Tekhnicheskoi Fiziki, No. 2, pp. 60-68, March-April, 1989. Original article submitted August 26, 1988.

0021-8944/89/3002-0223$12.50

TABLE 1

Calculation number	R	α_0	$E'(0)\cdot10^2$	T	$E'(T)\cdot10^5$	Method	τ	M	P
1	5 000	1,25	0,098	100	0,34	2(3)	0,25	9	31
2	5 000	1,25	0,88	150	3,4	2(3)	0,25	9	31
3	5 000	1,25	0,39	150	0,59	2(3)	0,25	9	31
4	5 000	1,25	9,8	600	0,3	2(2)	0,1	9	31
5	5 000	2,0	0,85	70	0,81	2(3)	0,25	9	31
6	10 000	1,25	0,25	250	1,2	2(3)	0,25	9	31
7	10 000	1,25	6,3	500	0,31	2(3)	0,25	9	31
8	10 000	2,0	0,34	250	0,016	2(3)	0,25	9	31
9	10 000	2,0	2,6	360	1,6	2(3)	0,1	9	31
10	5 000	0,5	0,4	250	2,1	1	0,1	33	33
11	5 000	0,3	0,22	250	1,2	1	0,1	33	33
12	5 000	0,3	0,8	350	0,81	1	0,1	33	33
13	5 000	0,3	3,0	500	3,2	1	0,025	33	33
14	5 000	0,15	0,48	250	5,0	1	0,1	33	33
15	10 000	0,3	0,42	250	4,6	1	0,1	33	33
16	10 000	0,15	1,9	600	12,9	1	0,1	33	33

lent flows observed in experiment. Two-dimensional and three-dimensional perturbations will be considered, periodic along the homogeneous coordinates x, y with periods $X = 2\pi/\alpha_0$, $Y = 2\pi/\beta_0$. The numerical solution of the Navier–Stokes equations written in Gromeki–Lamb form, will be performed by methods 1 and 2 (see [15, 16], respectively). In these methods the Galerkin method is used along the variables x, y with trigonometric polynomials as the base functions. In writing the solution for the normal variable z in method 1, Chebyshev polynomials of the first sort are used, while method 2 uses Jacobi polynomials $P_q^{(1,1)}(z)$.

In method 1, integration over time is performed by the partial step method. In the first and third partial steps the action of the term $[v, \mathrm{rot}\, v]$ is considered with second-order accuracy in t. To approximate the equations in z, the colocation method is used with nodes $z_\ell = \cos(\pi\ell/L)$, $\ell = 0, 1, \ldots, L$. In the second partial step the action of the total head gradient $\nabla\Pi$ and the dissipative term $\nu\Delta v$, are considered, using the incompressibility equation and the condition of adherence of the liquid to the channel walls. In this step the time approximation is carried out by an implicit technique, while the Petrov spectral method is used along z (for more detail, see [15]).

Method 2 utilizes a single step, and an implicit Crank–Nicholson type method of second-order accuracy is used to approximate the original equations over time, while along z a colocation method is used with nodes z_ℓ: $z_0 = -1, z_1, \ldots, z_{L-1}, z_L = 1$, where z_ℓ, $\ell = 1, \ldots, L-1$ are nulls of the Jacobi polynomial $P_{L-1}^{(1,1)}(z)$. Solution of the discrete problem is determined by iteration. We will note that, for this method, given the condition of convergence of the iterations, the discrete analogs of the laws of conservation of momentum and energy are satisfied exactly. This allows calculating turbulent flows in a plane channel with sufficiently large step in time [16].

Modeling of two- and three-dimensional pressure head-free flows was performed at transitional Reynolds numbers. For the initial conditions a laminar flow was specified, upon which various finite amplitude perturbations were imposed. Method 1 or 2 was then used to calculate the evolution of the flow until its exit to steady state, i.e., to a secondary or laminar flow. Exit to a secondary regime was monitored by stabilization of the basic integral flow characteristics (friction coefficient, energy pulsations, etc.). We note that existence of a secondary flow implies instability of the laminar flow relative to finite perturbations.

3. The approach described above was used to systematically search for pressure head-free two-dimensional secondary flows in a plane channel at R = 5000 and R = 10,000. A series of calculations were performed for various intervals of flow periodicity and initial conditions. Characteristics of the two-dimensional calculations are presented in Table 1. The first series of calculations (Nos. 1-9) modeled evolution of finite perturbations with periodicity intervals $X \lesssim 2\pi$ ($\alpha_0 \gtrsim 1$ are short-wave perturbations). The initial perturbation used was that eigenfunction of the Orr–Sommerfeld equation boundary problem with the least attenuation. The initial amplitude of the velocity perturbation was varied from 5 to 35% of the wall velocity (Table 1 shows values of the perturbation energy E' at t = 0). In all these calculations complete attenuation of perturbations was found: in the final portion of the calculations pulsations decayed by linear theory, while the flow tended to a laminar

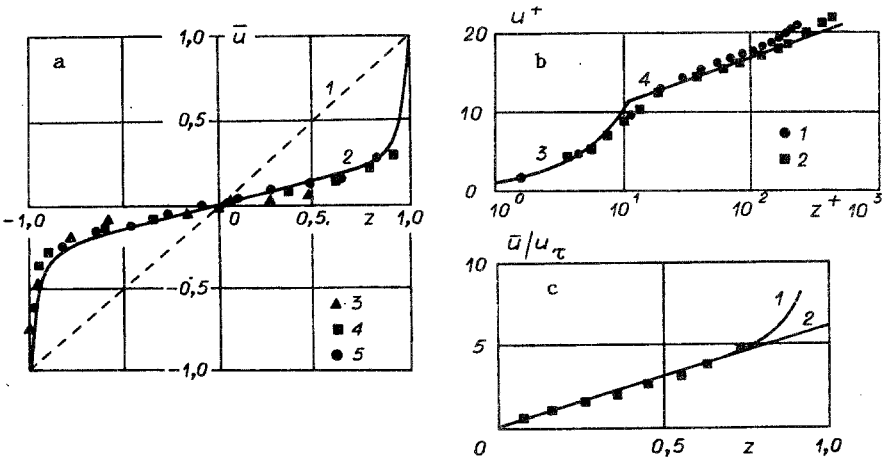

Fig. 1

Couette flow. Table 1 shows values of the perturbation energy E' at the end of each calculation, i.e., at time t = T. Also shown is the method used for the calculation, the time step τ, and the number of base functions used to represent the approximate solution in the variables x–M and z–P. For method 2, the number of iterations is given in parentheses.

In the subsequent series of calculations (Nos. 10-16) evolution of longwave perturbations ($\alpha_0 \leq 0.5$) was modeled for various initial amplitudes. The initial condition consisted of several Fourier harmonics in the representation of the approximate solution (in calculations 10-13 and 15, four harmonics; and in 14 and 16, eight). Damping of perturbations was also found in these calculations. However, it should be noted that in comparison to the shortwave case at an analogous or smaller initial perturbation amplitude attenuation of pulsations to the level where nonlinear interaction of the perturbations has practically no effect occurs over greater time intervals.

Thus, the calculations performed for various flow periodicity intervals and initial perturbation amplitudes did not reveal secondary (nonattenuating) two-dimensional flow regimes. It is clear that these studies are not exhaustive: only moderate Reynolds numbers were considered, the flow periodicity was varied over a relatively small range, only eigenfunctions of the linear problem were used as the initial condition, and, finally, a narrow class of perturbations was considered, with periodic dependence on the longitudinal coordinate. Nevertheless, the results of the present calculations, as well as the results of [7, 9] indicate that plane Couette flow, at least in the transition region, is stable relative to two-dimensional periodic finite amplitude perturbations. Apparently this is also true of arbitrary two-dimensional perturbations.

4. Three-dimensional flows were calculated for R = 750-5000; essentially shortwave perturbations were studied (see Table 2). In all calculations the approximate solution was represented by 9 × 9 Fourier harmonics in the variables x and y and 33 polynomials in z (for method 1, Chebyshev polynomials; for method 2, Jacobi polynomials). The integration step over time τ and the number of iterations for method 2 are shown in Table 2.

In the first calculation a three-dimensional flow with R = 5000 was modeled. For the initial condition the velocity field of the laminar flow was specified, with a finite-amplitude perturbation imposed thereon, in the form of a superposition of three eigenfunctions of the linear problem for wave numbers $(\alpha, \beta) = (\alpha_0, 0), (0, \beta_0), (\alpha_0, \beta_0)$. The energy of this perturbation E'(0) is given in Table 2. Flow evolution was calculated with method 2. In the initial stage there was an abrupt increase in the friction coefficient and total energy of the perturbations, after which, at $t \gtrsim 200$ a secondary flow regime was established with velocity profile characteristic of turbulent Couette flow. Thus, even in the first three-dimensional calculation, a secondary regime was obtained for head-free flow in a plane channel.

The next calculation was performed with the same parameters as the preceding one, but by method 1. For the initial condition the flow velocity field obtained at the end of calculation 1 was used. Flow evolution was calculated for a significant time interval for statistical processing of the results. Calculation of mean secondary flow characteristics

TABLE 2

Calculation number	R	α_0	β_0	$E'(0)\cdot10^2$	$T\cdot10^{-2}$	$\bar{E}\cdot10$	$\bar{E}'\cdot10^2$	$\bar{C}_f\cdot10^3$	Method	τ
1	5000	1,25	2	0,011	3	1,58	1,7	4,5	2(4)	0,1
2 *	5000	1,25	2	1,6	54	1,54	2,5	4,8	1	0,05
3 *	4000	1,25	2	2,5	20	1,73	2,3	5,4	1	0,05
4 *	2900	1,25	2	2,5	34	1,48	2,7	7,7	1	0,05
5 *	1450	1,25	2	2,6	16	1,45	2,6	9,5	1	0,05
6 *	1000	1,25	2	2,6	11	1,70	3,0	9,7	1	0,05
7 *	750	1,25	2	3,1	12	Exit to laminar regime			1	0,05
8	5000	0,5	2	2,6	12	1,79	2,7	4,7	1	0,05
9	5000	1,25	1	2,6	40	1,55	2,0	3,0	1	0,05
10	5000	3,125	5	2,6	5	0,93	1,2	4,2	2(3)	0,15
11	5000	5,0	8	2,6	6	0,92	1,2	3,6	2(3)	0,075
12	2900	1,25	3	2,8	16	1,40	2,5	7,1	1	0,05
13	2900	2,0	2	2,8	15	1,25	2,4	6,1	1	0,05

*In calculations marked by an asterisk the initial condition used was the flow velocity field obtained at the end of the preceding calculation.

$$\bar{f} = \langle f(\mathbf{x}, t)\rangle_{xyzt} = \frac{1}{2XY\Delta T}\int_D \int_{t_*}^{t_*+\Delta T} f(\mathbf{x}, t)\,dx\,dy\,dz\,dt,$$

$$D \equiv [\mathrm{x}:\ 0 \leqslant x \leqslant X,\ 0 \leqslant y \leqslant Y,\ |z| \leqslant 1]$$

was performed for various $t_* \gtrsim 10^3$ and intervals ΔT. It was thus established that change in the initial integration point t_* as well as increase in the interval $\Delta T \simeq 10^2$ leads to no noticeable changes in the mean secondary flow characteristics. This indicates that the secondary regime obtained is statically steady state. Table 2 presents values of the total perturbation energy $\bar{E}$, the pulsation energy $\bar{E}'$, and the friction coefficient $\bar{C}_f$. For comparison, we will note that in the experiments of [17] for turbulent Couette flow in a plane channel at R = 4930 a friction coefficient $C_f = 4.6\cdot10^{-3}$ was obtained.

In Fig. 1a, line 1 is the velocity profile of the laminar flow, line 2 is the mean velocity profile $u(z) = \langle u(x, t)\rangle_{xyt}$ of the three-dimensional secondary flow obtained in calculation 2. Other lines are experimental results at various Reynolds numbers: 3) R = 8200 [18]; 4) R = 17,000 [17]; 5) R = 28,500 [19]. In Fig. 1b, the velocity profile of the secondary flow is shown in semilogarithmic scale (points 1 correspond to colocation nodes), while points 2 are experimental results [20] for R = 9500. The mean velocity profile obtained in the calculation agrees quite well with experiment and the universal wall law: $u^+ = z^+$ (curve 3) for $z^+ \lesssim 10$ and $u^+ = 2.55\ln z^+ + 5.2$ (curve 4) for $z^+ \gtrsim 30$, where $u^+ = (1 - \bar{u})/u_\tau$, $z^+ = (1 - z)u_\tau/\nu$, $z \in [0, 1]$, $u_\tau = \left(\nu\left.\frac{d\bar{u}}{dz}\right|_{z=\pm1}\right)^{1/2}$. Moreover, in the flow core $|z| \lesssim 0.5$ the secondary flow velocity profile (Fig. 1c, curve 1) agrees with the velocity defect law, in which the variables used here can be written in the form $\tilde{u}/u_\tau = R_f z$, $R_f = 5.9$ (curve 2). It was shown in the experiments of [20] that with increase in R the coefficient R_f decreases, and for R = 9500, $R_f = 5.7$ (Fig. 1c, points).

Distributions of mean-square pulsations of each component of the velocity vector $v' = (u', v', w')$† for the three-dimensional secondary flow at R = 5000 and a turbulent flow at R = 9500 [20] are shown in Fig. 2a, b [1) u'/u_τ; 2) v'/u_τ; 3) w'/u_τ], $\tilde{z} = 1 - z$. Comparison of the graphs shows at least good qualitative agreement. In the central portion of the channel, $|z| \lesssim 0.5$, both calculation and experiment show a homogeneous distribution of the characteristics considered. The asymptotic dependence on the variable z in the vicinity of the channel wall for mean-square secondary flow velocity pulsations is shown in Fig. 2c. It is evident that the longitudinal and transverse components at $z^+ \lesssim 5$ have a linear dependence $u'/u_\tau = A_u z^+$, $v'/u_\tau = A_v z^+$ (curves 1 and 2), while for the normal component at $z^+ \lesssim 10$, the dependence is quadratic, $w'/u_\tau = A_w (z^+)^2$ (curve 3), while $A_u = 0.39$, $A_v = 0.22$, $A_w = 2.3\cdot10^{-3}$.

†$u' = (\langle\tilde{u}^2\rangle_{xyt})^{1/2}$; $\tilde{u}$ is the deviation of the longitudinal velocity component from the mean value; and v', w' are defined similarly.

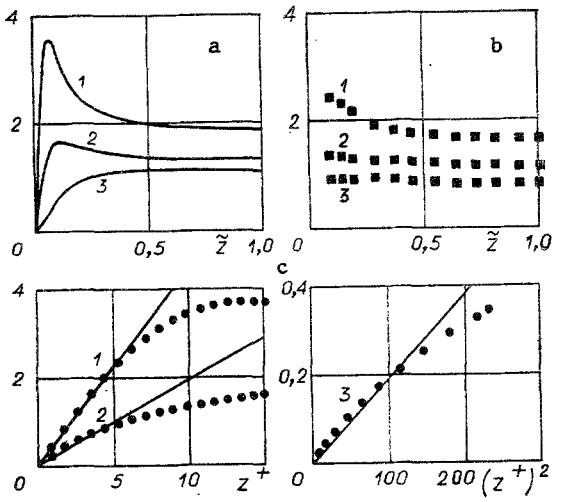

Fig. 2

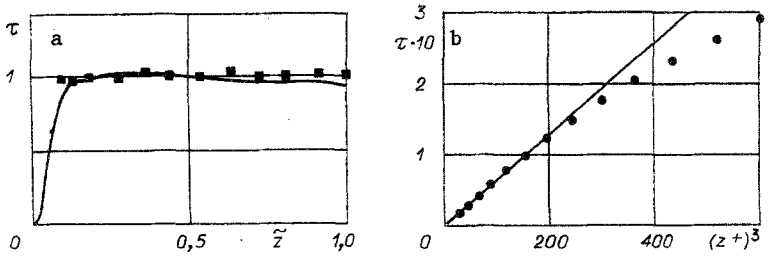

Fig. 3

Similar asymptotic dependences have been obtained in experiment [21] for developed turbulent Couette flow at R = 28,500. In this case, $A_u = 0.28$, $A_v = 0.08$, $A_w = 5 \cdot 10^{-3}$. Since the Reynolds numbers in the calculations and experiment differ significantly, we can speak only of qualitative agreement here.

The Reynolds stress $\tau(z) = -\langle uw \rangle_{xyt}/u_\tau^2$ for the secondary flow at R = 5000 is shown in Fig. 3a (line), while the points are experimental results [20] for R = 9500. The good agreement is evident. Figure 3b shows Reynolds stress in the vicinity of the channel wall. Here, at $z_+ \lesssim 5$ we have the asymptotic dependence $\tau = A_\tau (z_+)^3$, where $A_\tau = 4.9 \cdot 10^{-4}$. We note that use of numerical integration of the Navier–Stokes equations for pressurized turbulent flow in a plane channel at moderate Reynolds number has yielded similar expressions for the mean-square velocity pulsation and Reynolds stress, with $A_u = 0.36$, $A_v = 0.19$, $A_w = 8.6 \cdot 10^{-3}$, $A_\tau = 7.2 \cdot 10^{-4}$ [22].

Local mean distributions over z of the perturbation energy production $P(z) = \tau(z) \frac{d\bar{u}}{dz} \Big| u_\tau$ and dissipation $D(z) = -\nu \langle (\nabla \tilde{u})^2 + (\nabla \tilde{v})^2 + (\nabla \tilde{w})^2 \rangle_{xyt}/u_\tau^3$ for the secondary flow under consideration are shown in Fig. 4a (curve 1, P; curve 2, D). For perturbation energy production experimental results from [20] at R = 9500 are also shown (points). Figure 4b shows the function B(z) = P(z) + D(z), which characterizes the balance between energy production and dissipation by perturbations. In the vicinity of the channel wall energy dissipation takes place. In the range $0.62 \lesssim |z| \lesssim 0.96$ the energy transferred from the main flow to pulsations exceeds dissipation, with the generation maximum being reached near the walls $|z| \approx 0.94$. It is interesting that in the flow core $|z| \lesssim 0.6$ production and dissipation of energy by perturbations practically compensate each other.

Figure 5 shows turbulent viscosity $\nu_t = \tau(z) u_\tau \Big/ \frac{d\bar{u}}{dz}$ for the secondary flow at R = 5000 (line) and for a turbulent flow at R = 9500 [20] (points). In the central portion of the channel the ν_t values for the secondary flow are slightly less than the experimental ones. This can apparently be explained by the fact that the Reynolds numbers in the calculation and experiments differed by a factor of almost two times.

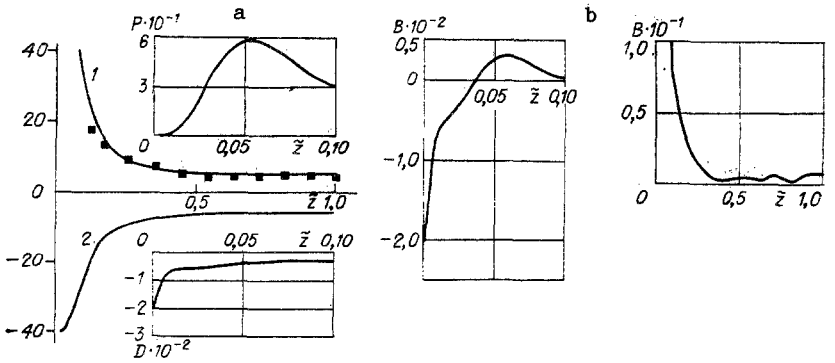

Fig. 4

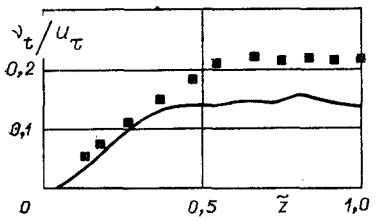

Fig. 5

In the subsequent calculations 3-7 (Table 2) the flow velocity field obtained at the end of the preceding calculation was used as the initial condition. Three-dimensional secondary flows were found for $R \gtrsim 10^3$. Secondary flows were not obtained for lower R in the periodicity interval $X = 2\pi/1.25$ and $Y = \pi$. Thus, instability of plane Couette flow relative to three-dimensional periodic finite amplitude perturbations at $R \gtrsim 10^3$ has been established. This result agrees fairly well with the experimental data of [3]. It is possible that consideration of long-wave perturbations might permit achievement of three-dimensional secondary flows at lower R.

Spatially periodic secondary flows in a plane channel for fixed Reynolds number form a two-parameter family of solutions of the Navier–Stokes equations, dependent on the wave numbers α_0, β_0. Calculations 8-13 (Table 2) were performed in order to clarify how change in α_0, β_0 affect the integral characteristics of the secondary flows. The initial conditions in these calculations were specified just as in calculation 1, with corresponding α_0, β_0 chosen in each case. In the calculations which considered the same number of base functions were used in representing the approximate solution as in the preceding calculations.

Comparison of calculations 2, 8, and 9 show that decrease in α_0 or β_0, corresponding to increase in the corresponding flow periodicity integrals, leads to some reduction in the friction coefficient and increase in the total perturbation energy. In turn, growth in α_0, β_0 (calculations 2, 10, 11 and 4, 12, 13) produce a reduction in both the friction coefficient and the total perturbation energy. It is clear that for each fixed value $R \gtrsim 10^3$ there exist α_0^*, β_0^* at which maximum friction is realized. Secondary flows with periodicity intervals $X^* = 2\pi/\alpha_0^*$, $Y^* = 2\pi/\beta_0^*$ can be termed limiting [15]. In the plane of the variables (R, C_f) the limiting secondary flows correspond to a curve which is the upper resistance boundary for the entire infinite set of secondary flows. Even approximate definition of this boundary is an extremely difficult problem. In the present study a coarse estimate was obtained for α_0^*, β_0^* only at R = 5000.

Calculations 10 and 11 were also performed with the goal of estimating the extent of the region of energy-containing vortices in wave number space. It developed that in the intervals $\alpha \in [5, 20]$, $\beta \in [8, 32]$ the harmonic energy decays by less than an order of magnitude. This indicates that for pressure head-free flow at transient Reynolds number (R = 5000) the given region is quite extended and its boundary is located outside the wave-number range of interest here, i.e., at $\alpha > 20$, $\beta > 30$. For comparison we note that in the case of pressurized secondary flow in a plane channel, also at transitional Reynolds number, in the segments $\alpha \in [1.3; 13]$, $\beta \in [2; 20]$ harmonic energy attenuation comprises more than two orders of magnitude. Apparently the elevation of mean-square velocity pulsations obtained

in the present study as compared to experiment is related to insufficient resolution of the region of energy-containing scales, i.e., in representing the approximate solution in the homogeneous variables x, y a small number of base functions was used.

In conclusion, we note that despite the relatively small number of degrees of freedom used to describe three-dimensional secondary flows, it has been possible to obtain the basic integral characteristics of turbulent Couette flow in a plane channel at transitional Reynolds numbers. At $R \gtrsim 10^3$ instability of laminar Couette flow relative to three-dimensional finite perturbations has been established. In addition no nonattenuating two-dimensional perturbations could be found at $R \lesssim 10^4$.

LITERATURE CITED

1. M. A. Gol'dshtik and V. N. Shtern, Hydrodynamic Stability and Turbulence [in Russian], Nauka, Novosibirsk (1977).
2. V. A. Romanov, "Stability of planoparallel Couette flow," Dokl. Akad. Nauk SSSR, 196, No. 5 (1971).
3. H. Reichardt, "On velocity distribution in rectilinear turbulent Couette flow," ZAMM, 36, special issue, 26 (1956).
4. H. J. Leutheusser and V. H. Chu, "Experiments on plane Couette flow," Proc. ASCE, J. Hydr. Div., 97, No. 9 (1971).
5. S. Kuwabara, "Nonlinear instability of plane Couette flow," Phys. Fluids, 10, No. 9, Part 2, Suppl. (1967).
6. T. Ellingsen, B. Gjevik, and E. Palm, "On the nonlinear stability of Couette flow," J. Fluid Mech., 40, No. 1 (1970).
7. T. Coeffe, "Finite amplitude instability of plane Couette flow," J. Fluid Mech., 83, No. 3 (1977).
8. A. L. Afendikov and K. I. Babenko, "The possibility of development of self-oscillating regimes in plane Couette flow," Dokl. Akad. Nauk SSSR, 252, No. 1 (1980).
9. M. Lessen and M. G. Cheifetz, "Stability of plane Couette flow with respect to finite two-dimensional disturbances," Phys. Fluids, 18, No. 8 (1975).
10. T. Herbert, "Finite amplitude stability of plane parallel flow," Proc. AGARD Symp. Laminar-Turbulent Transition, No. 224, paper 3 (1977).
11. S. A. Orszag and L. C. Kells, "Transition to turbulence in plane Poiseuille and plane Couette flow," J. Fluid Mech., 96, No. 1 (1980).
12. S. A. Orszag and A. T. Patera, "Secondary instability of wall-bounded shear flows," J. Fluid Mech., 128, 347 (1983).
13. B. Rummler and U. Breitschuh, "Calculation of turbuelent Couette flow by Galerkin approximation of the Navier–Stokes equation: Results and problems," ZAMM, 64, No. 10 (1984).
14. Y. Miyaka, T. Kajishima, and S. Obana, "Direct simulation of plane Couette flow at a transitional Reynolds number," JSME Int. J., 30, No. 259 (1987).
15. B. L. Rozhdestvenskii and I. N. Simakin, "Modeling turbulent flows in a plane channel," Zh. Vychisl. Mat. Mat. Fiz., 25, No. 1 (1985).
16. B. L. Rozhdestvenskii and M. I. Stoinov, "Algorithms for integration of the Navier–Stokes equations having analogs to the laws of conservation of mass, momentum, and energy," Preprint, Inst. Prikl. Mekh. Akad. Nauk SSSR, No. 119 [in Russian], Moscow (1987).
17. H. Reichardt, "Regularities of rectilinear turbulent Couette flow," Mitt. Max Planck Inst. für Ström., No. 22 (1959).
18. J. M. Robertson, "On turbulent plane Couette flow," Proc. 6th Midwestern Conf. Fluid Mech., Univ. Texas, Austin (1959).
19. M. M. M. El Telbany and A. J. Reynolds, "Velocity distributions in plane turbulent channel flows," J. Fluid Mech., 100, No. 1 (1980).
20. M. M. M. El Telbany and A. J. Reynolds, "The structure of turbulent plane Couette flow," Trans. ASME J. Fluids Eng., 104, 367 (1982).
21. M. M. M. El Telbany and A. J. Reynolds, "Turbulence in plane channel flows," J. Fluid Mech., 111, 283 (1981).
22. J. Kim, P. Moin, and R. Moser, "Turbulence statistics in fully developed channel flow at low Reynolds number," J. Fluid Mech., 177, 133 (1987).